


Cite this: *RSC Adv.*, 2023, 13, 35305

Insights into the use of two novel supramolecular compounds as corrosion inhibitors for stainless steel in a chloride environment: experimental as well as theoretical investigation

A. S. Fouda,^a S. E. H. Etaiw,^b A. M. Ibrahim^b and A. A. El-Hossiany^{a,c}

Novel supramolecular (SCPs) compounds such as: {[Ni (EIN)₄(NCS)₂]}, SCP1 and {[Co (EIN)₄ (NCS)₂]}, SCP2 have been studied using weight loss (WL) and electrochemical tests on the corrosion performance of stainless steel 304 (SS304) in 1.0 M hydrochloric acid (HCl) solution. The experimental results revealed that inhibition efficacy ($\eta\%$) rises with increasing concentrations of SCPs and reached 92.3% and 89.6% at 16×10^{-6} M, 25 °C, from the WL method for SCP1 and SCP2, respectively. However, by raising the temperature, $\eta\%$ was reduced. Polarization measurements (PDP) showed that the SCPs molecules represent a mixed-type. The SCPs were adsorbed on a SS304 surface physically, and the Langmuir adsorption isotherm was found to govern the adsorption process. The determination of thermodynamic parameters was carried out at various temperatures. Quantum chemical calculations were calculated to prove the adsorption process of SCP components, using the molecular dynamics (MD) simulations and electron density map. The inhibition performance of SCPs for SS304 dissolution in an acidic medium was proved to be excellent through FT-IR and AFM analysis. The results obtained from all measurements exhibit a high level of agreement with each other.

Received 30th October 2023
Accepted 23rd November 2023

DOI: 10.1039/d3ra07397a

rsc.li/rsc-advances

1. Introduction

The pickling process is an important step in the metal finishing industry. Hydrochloric acid is usually used as a method for achieving this goal.^{1,2} There are a number of financial and environmental risks associated with corrosion of metallic equipment in pickling.³ The high corrosion resistance of stainless steel makes it ideal for a variety of industrial applications. There is a strong passive film, which is formed by the mixture of iron oxide and chromium oxyhydroxide on the outer surface.⁴ Stainless steel surfaces can be reduced in corrosion resistance by chlorine-ion-containing solutions.⁵ It is true that part of the passive film is attacked by attacking ions, and other parts remain unharmed, so a galvanic couple forms on the steel surface, increasing corrosion. This is called pitting corrosion.⁶ The study of inhibitors to prevent corrosion of metals, especially stainless steel, has been conducted in the past few decades.^{7–9} Corrosion inhibitors are commonly used to defend these alloys from corrosion when operating or cleaning them.¹⁰ In the literature, there are numerous corrosion inhibitors for protecting metal specimens from acidic, salty, and similar harsh

environments.¹¹ The coordination complexes are excellent corrosion inhibitors because of their multifunctional structure, heteroaromatic chemistry, and richness in π -systems.¹² Because organic linkers are a common feature of these nanosized composites, researchers have been studying them for the past three decades owing to their ability to create a variety of structures.^{13,14} In various aqueous solutions, supramolecular complex composites have been demonstrated to inhibit corrosion of several metals.¹⁵ Aluminium terephthalates and their nanocomposite have been used as corrosion inhibitors against aluminium alloy corrosion in ethylene glycol solutions containing chloride ions, for instance.¹⁶ Nanoparticles improved inhibition efficiency from 86.52% to 90.8%, according to the results obtained. There have been reports of anticorrosion evidence for a variety of supramolecular chemical types. Based on the findings, this study suggests that corrosion inhibitors might be improved with a variety of benefits, including uniqueness and effectiveness. In this study, supramolecular nanosized complexes were synthesized by incorporating nickel and cobalt nanoparticles. Tests were conducted using 1.0 M HCl solution to assess the anticorrosion activity of the supramolecular nanoscale composite (SCP nanoscale).¹⁷ The porous and crystalline surfaces of these materials make them easy to adsorb.¹⁸ SCPs have been discovered to be efficient corrosion inhibitors due to their heteroaromatic ligands.¹⁹ This study examined synthesized and characterized SCP1 and SCP2 by

^aDepartment of Chemistry, Faculty of Science, Mansoura University, Mansoura 35516, Egypt. E-mail: asfouda@hotmail.com; Fax: +2 050 2202264; Tel: +2 050 2365730

^bDepartment of Chemistry, Faculty of Science, Tanta University, Tanta, Egypt

^cDelta for Fertilizers and Chemical Industries, Talkha, Egypt


single crystal structure and thermal analysis with a variety of methods including WL procedures, PDP and EIS tests. The inhibitors' effects on the SS304 surface were also determined using AFM analysis in HCl. Additionally, electron densities were calculated theoretically.

2. Experiments

2.1 Synthesis of inhibitors

2.1.1 Synthesis of $\{[\text{Ni}(\text{EIN})_4(\text{NCS})_2]\}$, SCP1. The SCP1 results by mixing amount of molar ratio 1:4:2 of Ni $(\text{NO}_3)_2 \cdot 6\text{H}_2\text{O}$ in 10 mL H_2O , EIN in 10 mL CH_3CN and KSCN in 5 mL water at ambient temperature. The resultant mixture was stirred gently for 20 min at room temperature. After about 3 days, green prismatic crystals of SCP1 were obtained. After filtration, washing with small quantities of cold H_2O and CH_3CN and overnight drying, (81%) of SCP1 had been obtained.²⁰ Elemental analysis yielded the following results for SCP1 ($\text{C}_{34}\text{H}_{36}\text{NiN}_6\text{O}_8\text{S}_2$): C, 52.39; H, 4.65; N, 10.78%. Found: C, 52.33; H, 4.68; N, 10.81%.

2.1.2 Synthesis of $\{[\text{Co}(\text{EIN})_4(\text{NCS})_2]\}$, SCP2. At ambient temperature, a solution containing 1 mmol of cobalt nitrate hydrate ($\text{Co}(\text{II})$, 0.291 g) dissolved in 20 mL of deionized water was slowly added to a stirred solution of 2 mmol (0.302 g) of EIN. The mixture obtained was stirred for a short duration, after which 5 mL of a water solution containing 2 mmol (0.194 g) of potassium thiocyanate was added drop by drop to the mixture, followed by additional stirring for a few minutes. Afterward, the solution was allowed to undergo gradual evaporation over a period of one month, resulting in the formation of pink crystals for SCP2 (436 mg, 63% yield).²¹ Elemental analysis yielded the following results for SCP2 ($\text{C}_{34}\text{H}_{36}\text{CoN}_6\text{O}_8\text{S}_2$): calculated: C, 52.37; H, 4.65; N, 10.78%. Experimental: C, 52.41; H, 4.68; N, 10.82% as shown in Table 1. All chemicals used are of BDH grade and used as received without further purification.

2.2 Specimens and test solutions

In this study, the sample of SS304 which used for WL and electrochemical measurements contains C 0.03%, Mn 2%, P 0.045%, N 0.01%, Si 75%, Cr 18–20%, Ni 8–12%, and Fe rest of the sample. Each test was repeated three times to ensure reliable and reproducible results. The corrosion tests in this study were conducted with a solution of hydrochloric acid (1.0 M HCl) obtained by diluting 37% HCl provided by Merck in bidistilled water. As an inhibitory solution, was diluted with 1.0 M HCl solution. A very small portion of dimethyl sulfoxide (DMSO) (5 mL) was added to the blank solution, and the compounds had excellent solubility in HCl solution. The various concentrations of SCPs were in the range of 7×10^{-6} M to 16×10^{-6} M and prepared from the stock solution (1×10^{-3} M) by dilution with 1 M HCl solution.

2.3 WL method

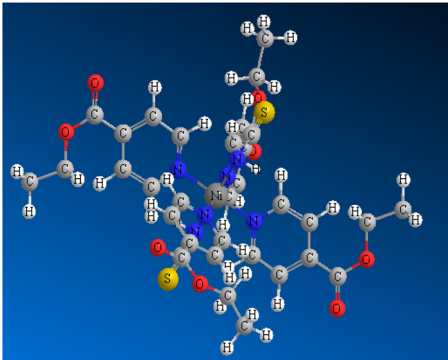
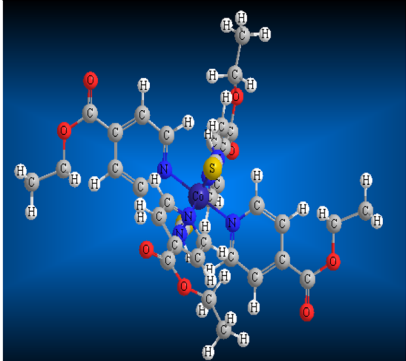
Based on the following procedures, the WL of SS304 samples was calculated: (1) weighing polished samples before dipping in the corrosive solution, (2) immersing them in corrosion inhibitors and without corrosion inhibitors, (3) removing, cleaning and drying them with cool air, (4) reweighing the required samples. Using WL, corrosion rate and inhibition efficiency (%) η_w) could be calculated as follows from eqn (1) and (2):²²

$$V = \frac{\omega_0 - \omega}{St} \quad (1)$$

$$\eta_w(\%) = \frac{V_0 - V}{V_0} \times 100 \quad (2)$$

The WL of SS304 without and with supramolecular (SCPs) inhibitors are represented by ω_0 and ω , the corrosion rate is denoted by V_0 while the exposed electrode surface area is denoted by S and t is the time of dipping (min). Thus, V_0 and V

Table 1 The molecular structure, weight, and formula of SCPs

SCPs	SCP1	SCP2
Mol. structure	$\text{Ni}(\text{EIN})_4(\text{NCS})_2$	$\text{Co}(\text{EIN})_4(\text{NCS})_2$
Mol. formula	$\text{C}_{34}\text{H}_{36}\text{N}_6\text{NiO}_8\text{S}_2$	$\text{C}_{34}\text{H}_{36}\text{N}_6\text{CoO}_8\text{S}_2$
Mol. weight	779.53	779.76
Structure		



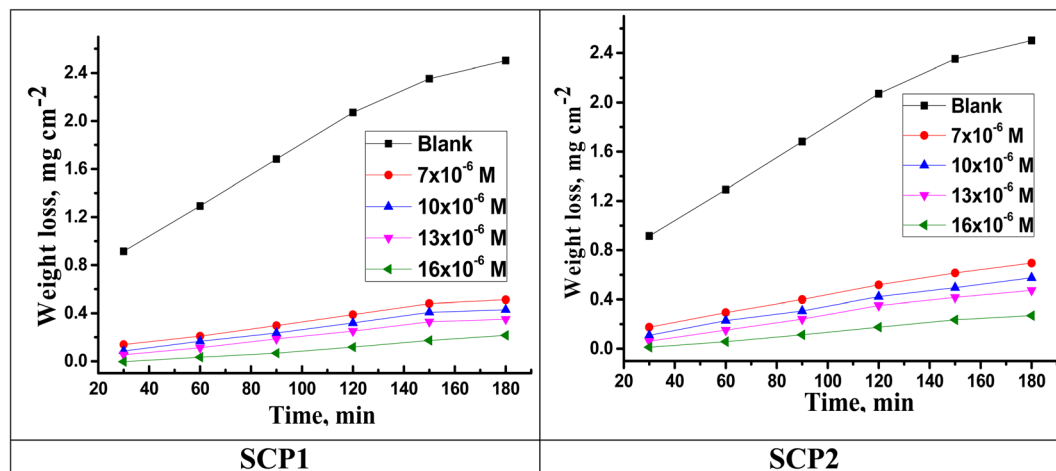


Fig. 1 Time-WL bends of SS304 in HCl with and without various concentrations of SCPs inhibitors at 25 °C.

correspond to the average corrosion rates of SS304 without and with SCPs inhibitors. Under every condition, seven parallel samples were used for the WL experiments.

2.4 Electrochemical techniques

An electrochemical reaction was studied with a Potentiostat/Galvanostat/ZRA and Gamry Instrument Series G 750™ analysis software. Three electrodes were used in all electrochemical testing. A reference electrode is made up of Ag/AgCl. Working electrode was SS304 specimen, with exposed area of 1 cm², and counter electrode was platinum electrode.²³ A 30 minute stabilization step was performed on the electrode immersed in the test solution before each electrochemical test. Tests performed on polarization were done at a scan speed of 0.2 mV s⁻¹ at ±250 mV vs. open potential circuit (OCP). AC signals of amplitude 10 mV at previous OCP potential were used for electrochemical impedance spectroscopy (EIS) in the frequency range 100 kHz to 10 mHz. As a mean of evaluating corrosion performance, Nyquist and Bode diagrams were used.

2.5 Theoretical studies

2.5.1 Quantum chemical calculations. The DMol3 module created in Materials Studio version 7.0 and Gaussian 0.9 software were used in theoretical simulations to evaluate the

relationship between the molecular structure and the reactivity of SCPs compounds.²⁴

2.5.2 Monte-Carlo simulations (MC). Using MC, the optimal positioning of SCPs inhibitors on the apparent of SS (111) was evaluated. It is believed that the SS (111) crystal surface used in this simulation is to its most stable according to the literature.^{25,26} The estimation module was initially used to carry out the geometrical optimization of water and the inhibitor molecule. Compass stimulation along with force field were implemented to SCP on SS (111) optimized surface. The substrate-adsorbate system configuration space was searched using the Monte-Carlo approach to identify low-energy adsorption sites where the temperature gradually decreases.²⁷

2.6 Surface morphology

Scanning probe microscopy (SPM) is used to study the SS304 surface using the Atomic force microscopy (AFM) apparatus (Model nanosurf c3000), with greater concentrations of the SCPs and without SCPs for 24 h, dipping period with confirmed resolution in the region of fractions of a manometer.²⁸ The AFM parameters are: mode: BudgetSensors Tap190AL-G Silicon, AFM probe with long Cantilever, resonant freq.: 190 kHz, force constant: 20 nN, coating: reflective Al, AFM tip shape: rotated, scan rate 1 Hz.

Table 2 $\eta\%$ at various concentrations of SCPs and altered temperatures for SS304 corrosion at 120 min in 1.0 M HCl solution

Comp.	Conc., $\times 10^6$ M	η (%)				
		25 °C	30 °C	35 °C	40 °C	45 °C
SCP1	7	85.0 \pm 0.1202	82.8 \pm 0.0667	81.0 \pm 0.133333	78.9 \pm 0.1732	78.4 \pm 0.1202
	10	87.2 \pm 0.0882	85.9 \pm 0.1732	84.3 \pm 0.145297	82.3 \pm 0.1155	81.6 \pm 0.1155
	13	89.5 \pm 0.2309	88.3 \pm 0.1764	86.6 \pm 0.088192	85.0 \pm 0.1000	85.3 \pm 0.0882
	16	92.5 \pm 0.1453	90.8 \pm 0.0882	88.9 \pm 0.066667	87.8 \pm 0.1453	87.0 \pm 0.1764
SCP2	7	74.7 \pm 0.1155	73.9 \pm 0.1202	72.5 \pm 0.233333	68.9 \pm 0.3283	68.2 \pm 0.1856
	10	80.1 \pm 0.0577	79.3 \pm 0.1155	76.9 \pm 0.11547	73.6 \pm 0.0882	72.6 \pm 0.2028
	13	83.7 \pm 0.1453	82.8 \pm 0.1202	81.0 \pm 0.24037	78.7 \pm 0.1155	78.1 \pm 0.1202
	16	86.4 \pm 0.1202	85.8 \pm 0.0882	84.1 \pm 0.176383	81.8 \pm 0.1528	80.3 \pm 0.1528



Table 3 Corrosion rate (k) at various concentrations of SCPs and altered temperatures for SS304 corrosion at 120 min in 1.0 M HCl solution

Comp.	Conc., $\times 10^6$ M	k				
		25 °C	30 °C	35 °C	40 °C	45 °C
Blank		0.133	0.163	0.216	0.441	0.564
SCP1	7	0.021 \pm 0.0013	0.028 \pm 0.0012	0.041 \pm 0.0017	0.093 \pm 0.0002	0.122 \pm 0.0012
	10	0.017 \pm 0.0015	0.023 \pm 0.0014	0.034 \pm 0.0013	0.078 \pm 0.0011	0.104 \pm 0.0017
	13	0.014 \pm 0.0017	0.019 \pm 0.0017	0.029 \pm 0.0015	0.066 \pm 0.0017	0.083 \pm 0.0011
	16	0.010 \pm 0.0014	0.015 \pm 0.0018	0.024 \pm 0.0014	0.054 \pm 0.0015	0.073 \pm 0.0012
SCP2	7	0.033 \pm 0.0015	0.042 \pm 0.0016	0.059 \pm 0.0017	0.137 \pm 0.0014	0.179 \pm 0.0013
	10	0.026 \pm 0.0013	0.033 \pm 0.0013	0.049 \pm 0.0016	0.116 \pm 0.0013	0.154 \pm 0.0017
	13	0.021 \pm 0.0012	0.028 \pm 0.0011	0.041 \pm 0.0014	0.093 \pm 0.0011	0.123 \pm 0.0016
	16	0.018 \pm 0.0010	0.023 \pm 0.0013	0.034 \pm 0.0011	0.080 \pm 0.0012	0.111 \pm 0.0012

2.7 Fourier transfer infrared spectroscopy (FTIR) analysis

The two synthesised SCPs compounds showed distinctive bands in the FTIR spectrum. "FTIR was carried out using a Thermo Fisher Nicolet IS10, USA spectrophotometer in the presence of (KBr)", which was used to verify and confirm the chemical structure for the substances.²⁹

3. Results and discussion

3.1 WL analysis

Fig. 1 shows the WL time curves for SS304 corrosion with and without different concentrations of SCPs inhibitors. As shown in the figure, the curves in the presence of different concentrations of SCPs are below the curves in their absence, indicating the adsorption of inhibitory molecules on the surface of SS304 and therefore ($\eta\%$) rises. Corrosion rate (k_{corr}) and inhibitor efficacy ($\eta\%$) of SCPs inhibitors were calculated for SS304 according to the eqn (1) and (2) under different temperatures, and are reported in Table 2. At high temperature, corrosion of SS304 increases under all conditions. According to this theory, the k_{corr} constant rises at a relatively higher temperature as shown in Table 3, which accelerates the electrochemical reactions.³⁰ The desorption of corrosion inhibitor

molecules may occur at high temperatures, accelerating further corrosion.³¹

3.2 Adsorption isotherm behaviour

Observation and analysis of the better adsorption isotherms of synthesized SCPs inhibitors using Langmuir, Flory-Huggins, Temkin, Frumkin, Freundlich type, and Kinetic model showed that the inhibition of adsorption behaviour on SS304 surfaces followed the Langmuir isotherm (Fig. 2)³² due to: (1) the straight lines with slopes close to unity on the plot of C/θ vs. C (concentration) at different temperatures; and (2) the good correlation ($R^2 > 0.99$), which was utilized to choose the isotherm that best suited the data. According to experimental data, SCPs adhered to this isotherm when adhering to the surface of SS304. According to this isotherm, there are no interactions between the adsorbed species and they each occupy a single location.³³ Eqn (3) provides the isotherm:³⁴

$$\frac{C_{\text{inh}}}{\theta} = \frac{1}{K_{\text{ads}}} + C_{\text{inh}} \quad (3)$$

K_{ads} represents the equilibrium constant of SS304 substrate adsorption, and C_{inh} represents the molar weight

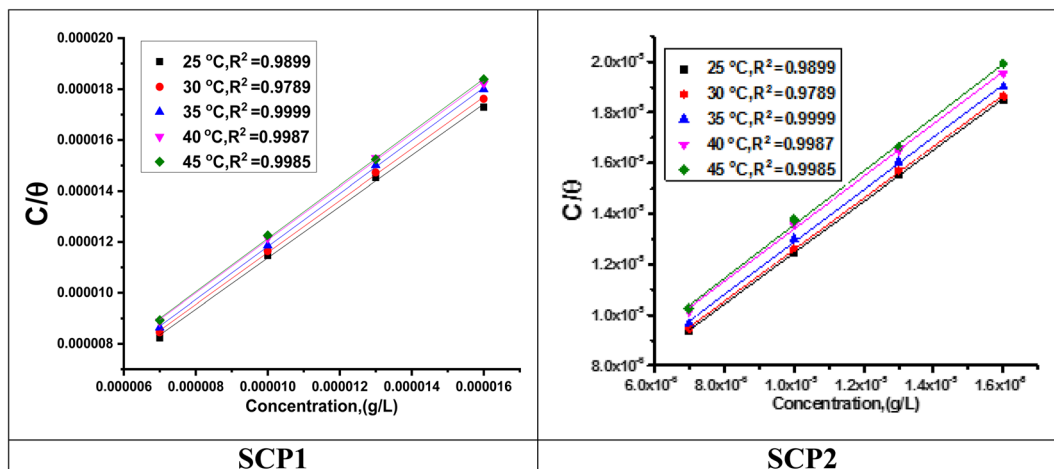
**Fig. 2** Langmuir diagrams of inhibitor SCP1 and SCP2 on SS304 surface in 1.0 M HCl.

Table 4 Thermodynamic parameters obtained from Langmuir adsorption isotherm

Inh.	Temp., °C	R^2	$K_{\text{ads}}, \text{M}^{-1}$	$-\Delta G_{\text{ads}}^\circ, \text{kJ mol}^{-1}$	$-\Delta H_{\text{ads}}^\circ, \text{kJ mol}^{-1}$	$-\Delta S_{\text{ads}}^\circ, \text{J mol}^{-1} \text{K}^{-1}$
SCP1	25	0.998	198	23.1	33.1	77.3
	30	0.997	166	22.9		75.7
	35	0.996	135	22.8		74.1
	40	0.999	105	22.6		71.9
	45	0.995	87	22.4		70.4
SCP2	25	0.998	143	22.2	31.8	74.5
	30	0.999	110	21.9		72.3
	35	0.998	88	21.7		70.5
	40	0.997	73	21.6		68.9
	45	0.999	62	21.5		67.6

of the synthesized SCPs inhibitors. The standard free energy of adsorption ($\Delta G_{\text{ads}}^\circ$) calculated from (K_{ads}) according eqn (4):³⁵

$$K_{\text{ads}} = \frac{1}{55.5} \times \exp\left(-\frac{\Delta G_{\text{ads}}^\circ}{RT}\right) \quad (4)$$

The water concentration at the interface among the SS304 and the solution is 55.5 (mol L^{-1}). Table 4 lists the $\Delta G_{\text{ads}}^\circ$ values. If $\Delta G_{\text{ads}}^\circ \geq -20 \text{ kJ mol}^{-1}$ and $\Delta G_{\text{ads}}^\circ \leq -40 \text{ kJ mol}^{-1}$, then according to literature it is physisorption or chemisorption.³⁶ The calculated $\Delta G_{\text{ads}}^\circ$ values are between -23.1 and $-21.5 \text{ kJ mol}^{-1}$. We can therefore conclude that the adsorption is mixed (physical or chemical) based on the obtained values of the $\Delta G_{\text{ads}}^\circ$ (between 20 and 40 kJ mol^{-1}),³⁷ but mainly physical based on the values of E_a^* and $\eta\%$. By using the Vant's Hoff equation, the enthalpy of adsorption ($\Delta H_{\text{ads}}^\circ$) was determined as follows from eqn (5):³⁸

$$\log K_{\text{ads}} = -\frac{\Delta H_{\text{ads}}^\circ}{2.303RT} + \text{constant} \quad (5)$$

Fig. 3 indicates plots of $\log K_{\text{ads}}$ and $1/T$. $\Delta H_{\text{ads}}^\circ$ can be determined from the line slope. The entropy ($\Delta S_{\text{ads}}^\circ$) of adsorption can be acquired by employing the following eqn (6):

$$\Delta S_{\text{ads}}^\circ = \frac{\Delta H_{\text{ads}}^\circ - \Delta G_{\text{ads}}^\circ}{T} \quad (6)$$

A negative value of $\Delta H_{\text{ads}}^\circ$ indicates an exothermic adsorption process. The $\Delta S_{\text{ads}}^\circ$ have negative sign, indicating that there is an increase in ordering during the process of adsorption as shown in Table 4.³⁹

3.3 Kinetic parameters

The relation between the k (corrosion rate) and temperature is expressed by the Arrhenius equation, eqn (7):⁴⁰

$$\ln k = \ln A - \frac{E_a^*}{RT} \quad (7)$$

where E_a^* is the activation energy. The plots of $\ln k$ vs. $1/T$ are illustrated in Fig. 4, from this plot, the values of E_a^* were computed and are inserted in Table 5. The increased E_a^* values in the presence of SCP1 and SCP2 were greater than that obtained in the blank. These findings indicate the adsorption of SCP1 and SCP2 on the SS304 surface, constructing a barrier to separate such surface from the corrosive solution.⁴¹ By stopping the charge/mass transfer interaction on the surface, the adsorbed layer shields the SS304 from strong acid assault.⁴²

The values of E_a^* were smaller than 80 kJ mol^{-1} that required for chemical adsorption, indicating that the kind of adsorption

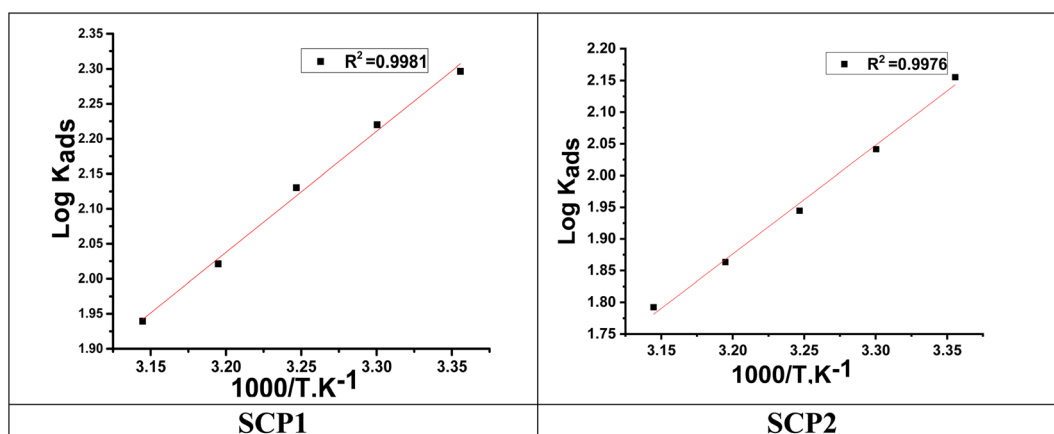


Fig. 3 The relation between $\log K_{\text{ads}}$ and $1000/T$ curve for the dissolution of SS304 in 1.0 M HCl in the presence of SCPs compounds.



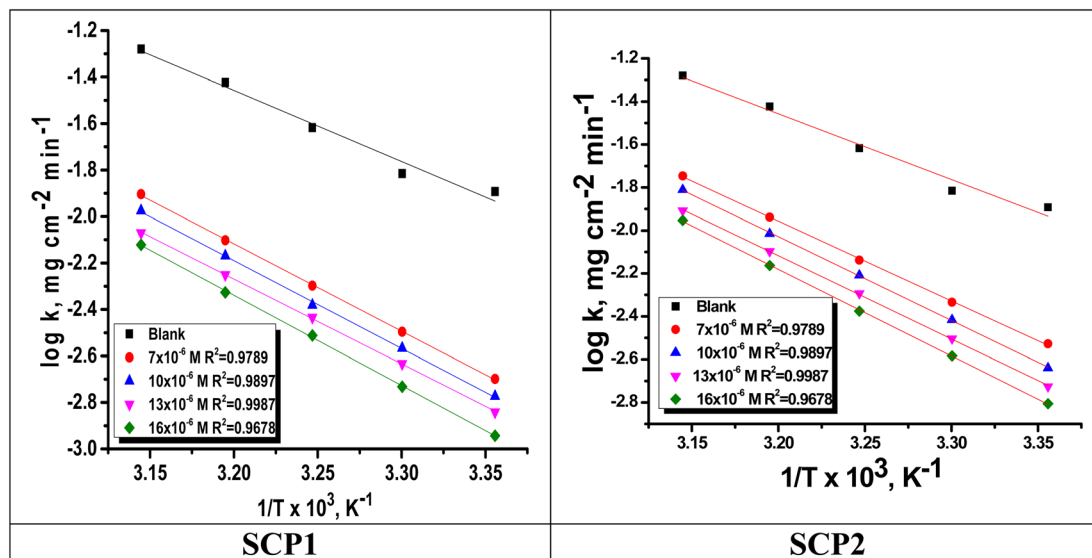


Fig. 4 Arrhenius bends for SCPs inhibitors corrosion in 1.0 M HCl solution and with: SCP1 and, SCP2.

was physical.⁴³ The dissolution of SS304 shows endothermic properties, as indicated by the positive ΔH^* readings, suggesting that the presence of SCPs reduces the corrosion rate.

The outcome data (ΔH^* and ΔS^*) are evaluated *via* eqn (8):^{44,45}

$$\ln\left(\frac{k}{T}\right) = \left(\ln\frac{R}{Nh} + \frac{\Delta S^*}{R}\right) - \frac{\Delta H^*}{R} \frac{1}{T} \quad (8)$$

The plots of $\ln\left(\frac{k}{T}\right)$ vs. $\frac{1}{T}$ were set to straight Fig. 5. The evaluated values of ΔH^* and ΔS^* are listed in Table 6. The positive ΔH^* values obtained suggest that the dissolution process of SS304 is endothermic in nature and the ΔH^* values increase with increasing SCPs concentration, suggesting that the dissolution reaction of SS304 to a higher concentration requires more energy. The presence of SCPs in the inhibited solution reduces the freedom of motion of inhibitor molecules, as shown by the negative activation entropy (ΔS^*) signals. The activated complex also exhibits a association rather than dissociation in the rate-determine step, demonstrating the occurrence of a successive arrangement from the transition of

the reactants to the activated complex.^{46,47} The results obtained allow us to verify the well-known thermodynamic relationship between E_a^* and ΔH^* (eqn (9)), which characterizes a mono-molecular reaction:⁴⁸

$$E_a^* - \Delta H^* = RT \quad (9)$$

The calculated value (2.50 at 298 K) is too close to the value estimated in Table 6. The inhibitor therefore acts on E_a^* and ΔH^* in the same way.

3.4 Electrochemical analysis

3.4.1 PDP studies. A plot of the PDP tests was used to determine the inhibitory mechanisms of SCPs compounds. SCP1 and SCP2 concentrations were determined using Tafel polarization curves, which are shown in Fig. 6. The deduced electrochemical parameters from Tafel plots such as corrosion potential (E_{corr}), Tafel slopes (β_c and β_a), corrosion current density (i_{corr}), and the corresponding inhibition efficiency (η_{Tafel}) are shown in Table 6. Polarization curve analysis shows that the introduction of SCPs inhibitors into the 1.0 M HCl solution resulted in lower anodic and cathodic current densities

Table 5 Activation parameters of the dissolution of SS304 in 1.0 M HCl with and without SCPs at 25–45 °C

Inhibitor	Conc., $\times 10^6$ M	$-E_a^*$, kJ mol ⁻¹	ΔH^* , kJ mol ⁻¹	$-\Delta S^*$, J mol ⁻¹ K ⁻¹
Blank	0.0	66.4 ± 0.2078	63.9 ± 0.2071	78.2 ± 0.1341
SCP1	7	78.1 ± 0.1202	75.6 ± 0.0882	52.7 ± 0.1453
	10	79.8 ± 0.0882	77.3 ± 0.1528	53.8 ± 0.1202
	13	81.1 ± 0.2603	78.6 ± 0.2028	52.9 ± 0.2028
	16	82.9 ± 0.2887	80.4 ± 0.1202	59.1 ± 0.1528
SCP2	7	76.9 ± 0.2309	74.4 ± 0.1155	53.9 ± 0.2028
	10	78.2 ± 0.1528	75.7 ± 0.1764	54.6 ± 0.2082
	13	78.8 ± 0.1856	76.3 ± 0.2404	42.9 ± 0.1764
	16	81.1 ± 0.1732	78.6 ± 0.1732	48.6 ± 0.2404



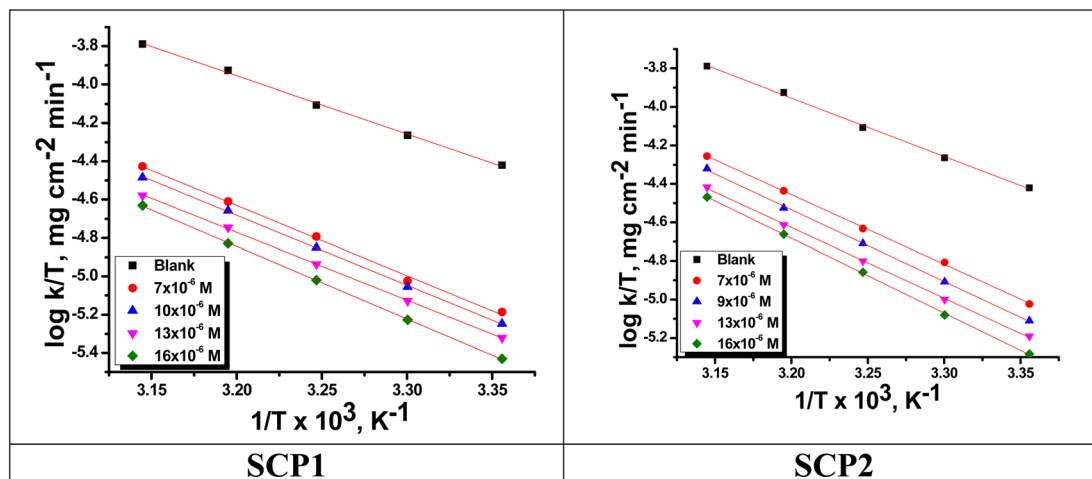


Fig. 5 $\log\left(\frac{k}{T}\right)$ vs. $\frac{1}{T}$ plots for SCPs inhibitors corrosion in 1.0 M HCl solution and with: SCP1 and, SCP2.

for both anodic and cathodic processes. Therefore, the dissolution reactions in the anodic branch are delayed, hydrogen gas accumulates when the cathodic branch is activated, and SS304 corrosion is inhibited. The cathode-panel lines in Fig. 6 are formed in parallel, indicating that the addition of SCPs has no effect on the hydrogen evolution mechanism, and the reduction of hydrogen ions on the surface of SS304 is mainly through the hydrogen transfer mechanism charge.⁴⁹ According to this study, the absence of important fluctuations in E_{corr} values in the presence of SCPs compared to E_{corr} in the absence of SCP (10–17) mV indicates that SCPs are mixed inhibitors (anode-cathode).⁵⁰ As a result, the cathodic evolution of hydrogen was not significantly affected by the adsorbed molecules. Based on these results, it appears that increasing inhibitor concentration decreases current density and thus, corrosion rate due to the adsorption of SCPs molecules on SS304 surface, consequently enhances the $\eta\%$. These data suggest that an inhibitory effect exists.

3.4.2 EIS studies. For the analysis of electrochemical systems, EIS stands out as one of the most useful techniques (EIS). The Nyquist and Bode plots shown in Fig. 7 and 8, respectively illustrate surface characteristics of SS304 samples and dynamics electrochemical processes in an uninhibited solution of 1.0 M HCl, and at various concentrations of **SCP1** and **SCP2**. A charge transfer process is implied by the half-loop

Nyquist curves of the studied system with one time constant. Blank loops have a smaller diameter than inhibitor loops, and loop forms are not altered as inhibitor concentration increases. According to these results, the corrosion process is not modified, and a covering film may form on the surface of the stainless steel due to adsorption of inhibitors.⁵¹ Thus, corrosion reactions are governed by the process of charge transfer between metals and solutions. The electrode surface may be protected from acidic solution by an adsorbed inhibitor film (**SCP1** and **SCP2**), which slows contact with the acidic solution and inhibits SS304 dissolution. An evident time constant is observed in the Bode diagram Fig. 8. A frequency dispersion induced deviation has been avoided by replacing the ideal capacitance of double layer (C_{dl}) with the CPE in the equivalent circuit". This formula (eqn (10)) defines the CPE parameter as the flattened nature of Nyquist spectra allows us to have a more precise fit.⁵²

$$Z_{\text{CPE}} = Q^{1-n} \times (i \times \omega)^{-n} \quad (10)$$

where the parameters (Q , i , ω , n) are respectively in this order, CPE constant, imaginary number with $i^2 = -1$, the angular frequency with $\omega = 2 \times \pi \times f$ and CPE exponent lies within a range of -1 to 1 . CPE in Fig. 9 explains the circuit components based on the value n . Thus, for exponent value n equal to 1 , 0 ,

Table 6 PDP data for the dissolution of SS304 in 1.0 M HCl solution in the absence and presence of the SCPs inhibitors at 25 °C

Inh.	[Inh.] $\times 10^6$ M	$-E_{\text{corr}}$, mV	i_{corr} , $\mu\text{A cm}^{-2}$	$-\beta_{\text{c}}$, mV dec $^{-1}$	β_{a} , mV dec $^{-1}$	k , mm	θ	η (%)
SCP1	0.0	138 \pm 0.2431	795 \pm 0.1732	133	63	415	—	—
	7	131 \pm 0.2431	201 \pm 0.2028	124	57	293	0.747	74.7
	10	126 \pm 0.1742	158 \pm 0.1155	143	51	231	0.801	80.1
	13	118 \pm 0.2102	142 \pm 0.2603	121	41	208	0.821	82.1
	16	128 \pm 0.2010	79 \pm 0.1764	127	45	116	0.901	90.1
SCP2	7	132 \pm 0.1753	235 \pm 0.2028	101	60	342	0.704	70.4
	10	122 \pm 0.1208	163 \pm 0.1732	126	52	237	0.795	79.5
	13	117 \pm 0.2128	149 \pm 0.1453	154	58	218	0.813	81.3
	16	130 \pm 0.2127	141 \pm 0.1732	116	50	205	0.823	82.3

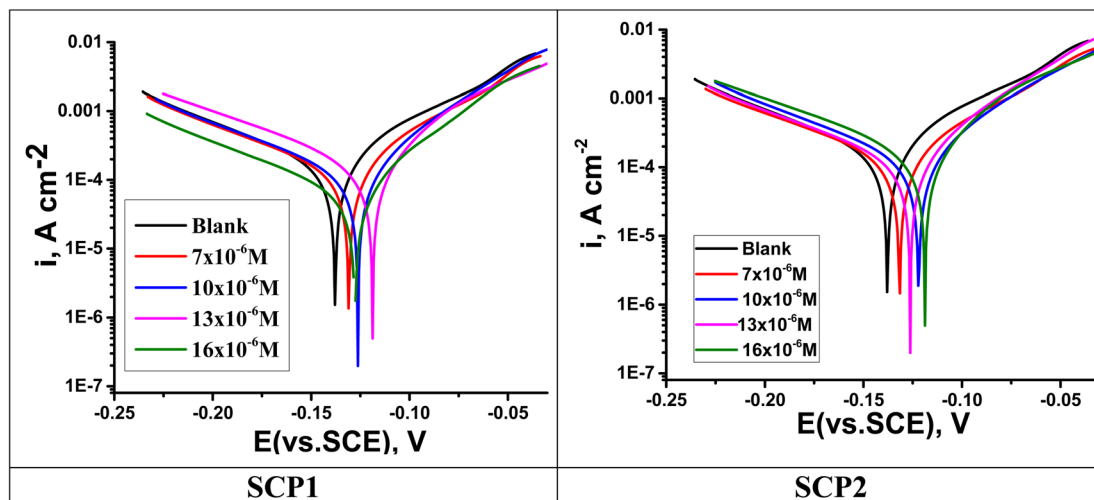


Fig. 6 PDP curves for SS304 obtained at 25 °C in 1.0 M HCl solution containing altered concentrations of SCP1 and SCP2.

0.5, or 1, the following values are given: inductance, resistance, and Warburg impedance". n is a measure that reveals a deviation from the ideal behaviour. The following criteria were used to determine which SCPs suited best: the tolerated errors of the elements in fitting mode (5%), as well as the chi-square error, were both small ($\chi^2 < 10^{-3}$). Table 7 lists the SCPs parameters' numerical values. The Y_0 estimate for the reference electrolyte is higher than that for the inhibited electrolyte. This suggests that SCPs molecules interact with the electrode surface, thereby limiting the destruction of exposed electrode sites. The next formula (eqn (11)) was used to calculate the double layer capacitances, C_{dl} , of a circuit containing a CPE.⁵³

$$C_{dl} = (Q \times R_p^{1-n})^{1/n} \quad (11)$$

where, Q is the magnitude of the CPE, i indicate the imaginary number of CPE, ω is the angular frequency ($\omega_{\max} = 2\pi f_{\max}$), f_{\max} is the maximum frequency, and n is the empirical constant. In fact, the increase in R_p value and the concomitant decrease in

C_{dl} with the increase in SCPs concentration suggest that the corrosive ions and water molecules coming from the surface of the substrate are replaced by inhibitory molecules, which increases the thickness by double electrical power layer and reduces the local dielectric constant and this is a sign that SCPs were acting at the SS/acid interface.⁴⁸ However, the increase in n value after the addition of SCP in the 1 M HCl electrolyte is larger than that in the reference electrolyte, which can be interpreted as a certain reduction in surface heterogeneity.⁵⁴ In uninhibited and inhibited solutions, the polarization resistance R_p can be used to calculate SCPs inhibition efficiency (eqn (12)).⁵⁵

$$IE_{EIS}(\%) = \frac{R_{p(inh)} - R_p}{R_{p(inh)}} \times 100 \quad (12)$$

Table 7 displays the values of the EIS's fitted parameters. SCP1 and SCP2 increase the R_{ct} much more than uninhibited solutions. Observations suggest that SCP1 and SCP2 molecules

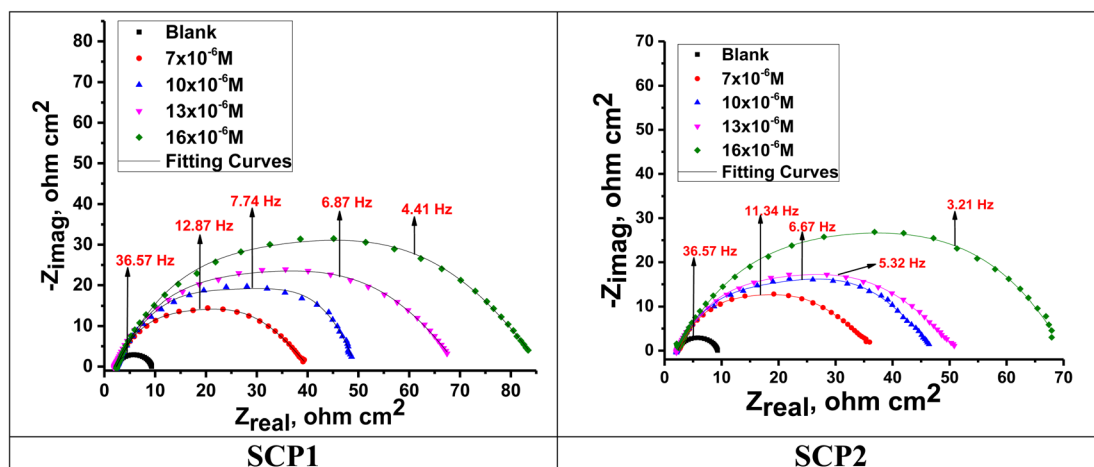


Fig. 7 Nyquist bends for SS304 in 1.0 M HCl without and with altered concentrations of inhibitors SCP1 and SCP2 at 25 °C.



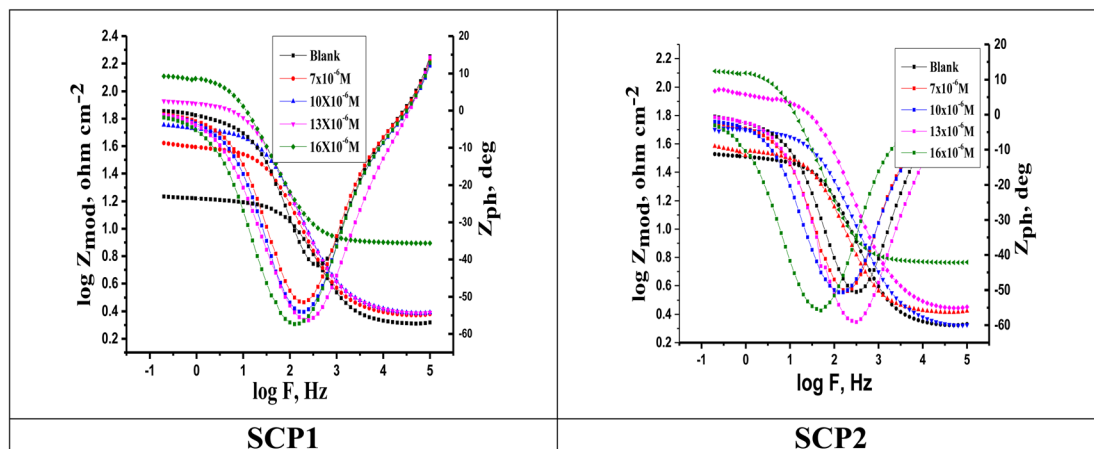


Fig. 8 Bode plots for SS304 in 1.0 M HCl attendance and without altered concentrations of inhibitors SCP1 and SCP2 at 25 °C.

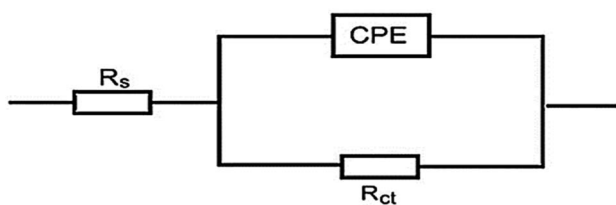


Fig. 9 Electrical circuit for experimental data fitting of SCP1 and SCP2.

adhere to SS304 surfaces, forming a protective layer.⁵⁶ The outcomes from Table 7 indicate a further increase in inhibition efficiency was observed for both SCP1 and SCP2, respectively, at 92.3% and 89.6%.

3.5 Theoretical analysis

3.5.1 Quantum chemical parameters. The lower energy band gap value, which is represented in the energy band gap ΔE_g ($\Delta E = E_{\text{HOMO}} - E_{\text{LUMO}}$), indicates that organic molecules are highly reactive and exhibit excellent corrosion behaviour on the surface of SS304. An analysis of the impact of SCPs molecule's orientation on inhibition performance was conducted using density functional theory (DFT). As shown in Fig. 10, the optimized geometry, HOMO surface, and LUMO surface of studied inhibitors can be found. The parameters HOMO (E_{H}), LUMO

(E_{L}), and dipole moment (μ) for MOFs gradients were directly obtained from DFT (Table 8). Eqn (13)–(18) were used to calculate the energy gap (ΔE), electronegativity (χ), global hardness (η), global softness (σ), the fraction of electron transfer (ΔN) and back-donation ($\Delta E_{\text{backdonation}}$), was calculated as Koopmans's theorem⁵⁷ from the next balance:

$$\mu = -\chi = -\frac{I_{\text{p}} + E_{\text{A}}}{2} \quad (13)$$

$$\chi = \frac{I_{\text{p}} + E_{\text{A}}}{2} \quad (14)$$

$$\eta = \frac{I_{\text{p}} - E_{\text{A}}}{2} \quad (15)$$

$$\sigma = \frac{1}{\eta} \quad (16)$$

$$\omega = \frac{\mu^2}{2\eta} \quad (17)$$

$$\Delta E_{\text{backdonation}} = -\frac{\eta}{4} \quad (18)$$

Numerous articles^{58,59} have discussed how higher values of E_{HOMO} and lower values of E_{LUMO} determine the greater electron-donating and accepting abilities of an inhibitor.

Table 7 EIS for SS304 after immersion in 1.0 M HCl in the presence of altered concentrations of SCP1 and SCP2

Comp.	Conc., $\times 10^6$ M	R_{ct} , $\Omega \text{ cm}^2$	C_{dl} , $\times 10^4$, $\mu\text{F cm}^{-2}$	n	Y_0 , $(\mu\Omega^{-1} \text{ s}^n \text{ cm}^{-2}) \times 10^{-6}$	Θ	η (%)	Goodness of fit χ^2
Blank	0.0	6.7 ± 0.1456	147 ± 0.2775	0.915	164	—	—	8.55×10^{-3}
SCP1	7	40.8 ± 0.2516	122 ± 0.2309	0.939	152	0.836	83.6	6.57×10^{-3}
	10	48.8 ± 0.1527	104 ± 0.1201	0.948	145	0.863	86.3	6.54×10^{-3}
	13	63.2 ± 0.2728	78 ± 0.2333	0.958	115	0.894	89.4	5.74×10^{-3}
	16	86.9 ± 0.2333	67 ± 0.1855	0.959	105	0.923	92.3	4.89×10^{-3}
SCP2	7	37.3 ± 0.1808	131 ± 0.2496	0.913	160	0.820	82.0	4.32×10^{-3}
	10	43.1 ± 0.1201	118 ± 0.1732	0.914	151	0.845	84.5	5.77×10^{-3}
	13	47.9 ± 0.2309	86 ± 0.1527	0.921	126	0.860	86.0	7.12×10^{-3}
	16	64.7 ± 0.1763	71 ± 0.2185	0.936	113	0.896	89.6	6.66×10^{-3}

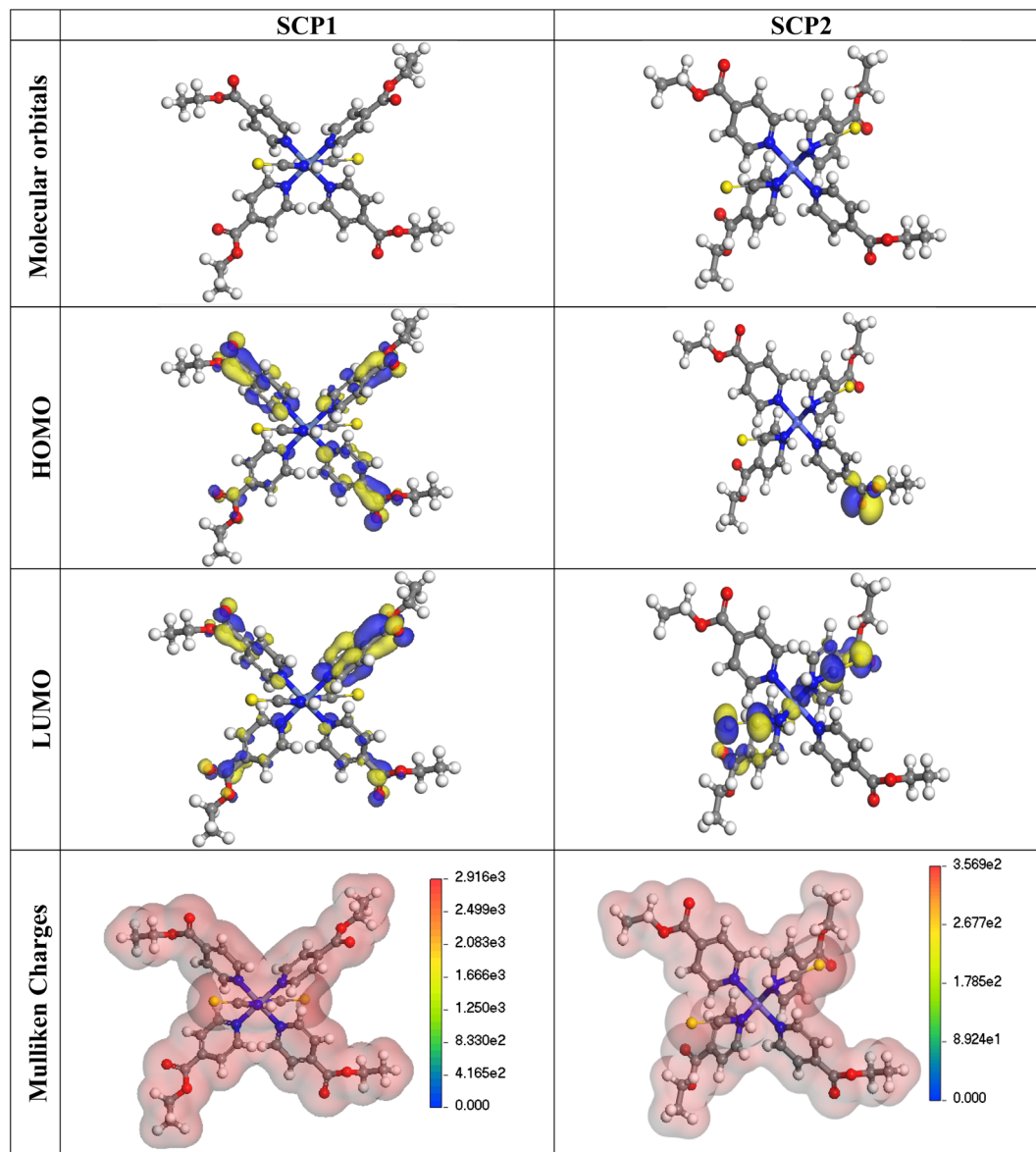


Fig. 10 The optimized geometrical structure, (HOMO), and (LUMO) of the tested SCPs at DMol3.

Table 8 Quantum chemical data for SCPs under study

Compound	SCP1	SCP2
$-E_{\text{HOMO}}$, eV	4.999	6.027
$-E_{\text{LUMO}}$, eV	3.968	4.183
ΔE , eV	1.031	1.844
I_{p} , eV	4.999	6.027
E_{A} , eV	3.968	4.183
χ , eV	4.4835	5.105
η , eV	0.5155	0.922
σ , eV	1.939864	1.084599
ω	19.49735	14.13288
ΔN	2.440834	1.027657
$\Delta E_{\text{back-donation}}$	-0.12888	-0.2305
Dipole moment (Debye)	12.87	18.53

Inhibitors are more reactive when a lesser value of ΔE is present. In this instance, **SCP1** ΔE value is lower while higher values for **SCP2**. In comparison to SCPs molecules, these values suggest that **SCP1** molecule has a high degree of reactivity. Metals and inhibitors can be understood using the number/fraction of electron transfer (ΔN). If the ΔN value of an inhibitor is higher, it is found to have a stronger capability of donating electrons to metallic surfaces. Compared to SCPs molecules, **SCP1** exhibits greater amounts of ΔN in the gaseous phase, indicating that **SCP1** exhibits a stronger inhibitory effect.

3.5.2 Monte Carlo (MC) simulation. MC modeling is a good method for calculation of the most stable adsorption conformations of a SCPs. Fig. 11 illustrates the simulation findings for the investigated SCP, which are described in Table 9. Fig. 11 depicts the adsorbed molecule's most favorable confirmation on the SS metal surface (111). Furthermore, the molecules stated are



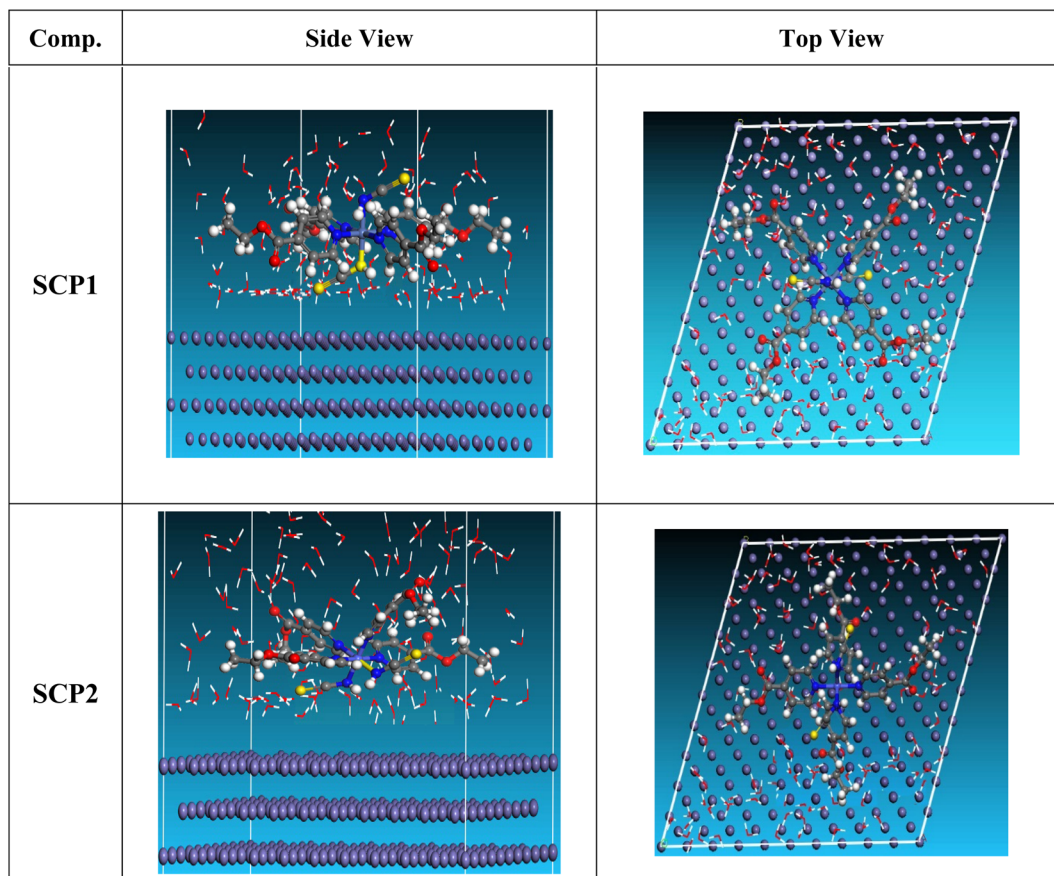


Fig. 11 Adsorption shapes of the SCPs molecules on SS304 surface.

adsorbed on the metal surface from the motive, which is rich in inhibitory molecule electrons. The interactions between the occupied orbitals of the examined SCPs and the vacant orbitals of SS (111), which are reflected by energy adsorption values (E_{ads}), of the rigid energy (E_{rigid}), of the deformation energy (E_{def}), and energy ratio values (dE_{ads}/dN_i) of the inhibitors, which is equivalent to the energy of substrate–adsorbate configurations where one of the adsorbate components has been removed are collected in Table 9. Adsorption energy values that are more negative indicate a highly stable and strong connection between adsorbed molecules and metal. When two materials are mixed during the adsorption process, an electron, ion, or molecule (adsorbent) is attached to the solid surface, adsorption energy is defined as declining energy.⁶⁰ As shown in Table 9, the greater adsorption energy of SCP1 rather than SCP2 on the hardened Fe surface predicts heavy adsorption of SCP molecules, forming a stable adsorbed layer that protects the

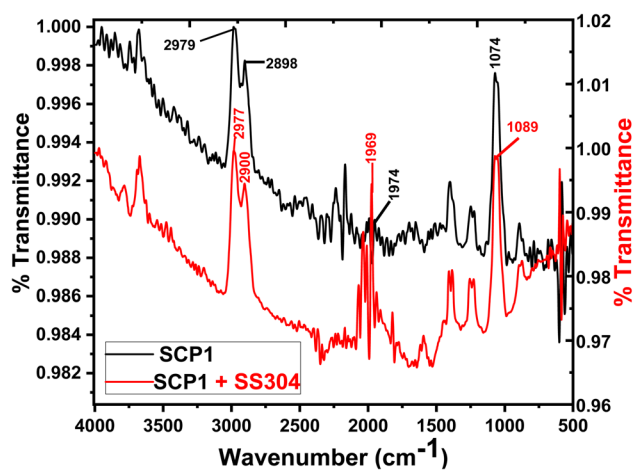


Fig. 12 FTIR spectra of pure inhibitors and SS304 following a 24 hour exposure in an acidic environment with 16×10^{-6} M of SCP1 at 25 °C.

Table 9 MC parameters of adsorption of SCPs molecules on SS304 (111) surface

Structures	Adsorption energy	Rigid adsorption energy	Deformation energy	Compound dE_{ad}/dN_i	H ₂ O dE_{ad}/dN_i
SS304 (111)/inhibitor SCP1/H ₂ O	−3332.977	−3522.547	189.57	−265.58	−11.08
SS304 (111)/inhibitor SCP2/H ₂ O	−3178.027	−3347.687	169.66	−223.79	−9.87



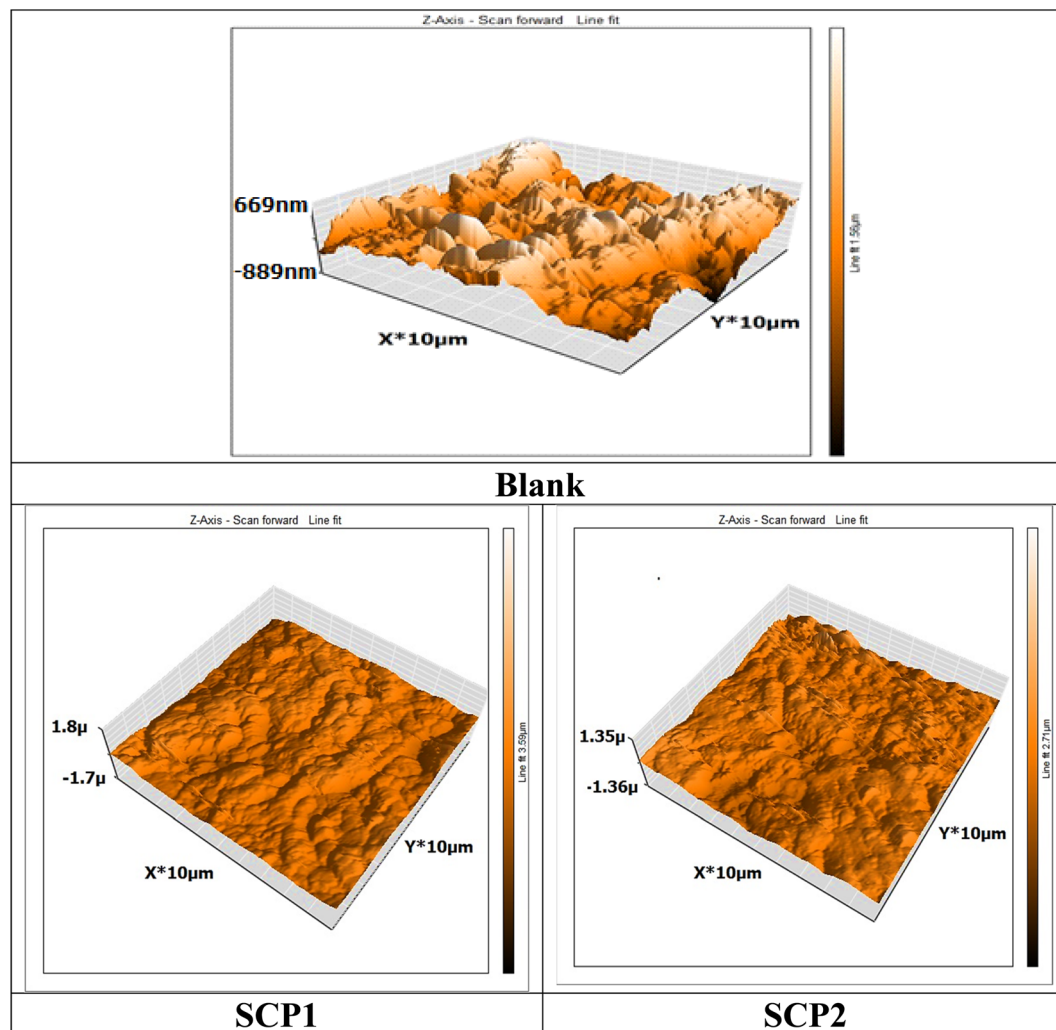


Fig. 13 3D AFM morphology of SS304 samples surface without and with SCPs compounds.

iron from decomposition. The tabulated adsorption energies are -3332.977 and -3178.027 kcal mole $^{-1}$ for **SCP1**, **SCP2** respectively. The outputs shows that the two inhibitors are efficient adsorptive inhibitors taking in respect that the better one is **SCP1** which is attuned with the experimental results". Based on theoretical modeling it's obvious that SCPs based proved to be powerful inhibitors for the SS304 which is confirmed by experimental and spectral investigation.

3.6 FT-IR spectroscopy

The inhibitors on the SS304 surface were detected by infrared spectroscopy in 1.0 M HCl in Fig. 12. On the surface of the SS304 specimen, the FTIR spectra of the pure inhibitors were compared to those of the adsorbed SCPs inhibitors. The inhibition spectrum and the adsorbed molecules of **SCP1** on the surface of SS304 metal shows that certain peaks are moving or disappearing, while others become less prominent. This suggests the **SCP1** compound is well absorbed by SS304 surfaces, which causes inhibition.⁶¹ At $(2979, 2977)$ cm $^{-1}$ are linked to the extension of chemical groups involving $(-C-H)$

stretching group". The spectral regions at $(2898, 2900)$ cm $^{-1}$ are linked to the extension of chemical groups involving $(-CH_2)$ aliphatic stretching group. Furthermore, the spectral feature at $(1669, 1674)$ cm $^{-1}$ is allocated to the stretching vibrations of specific $(C=O)$ bonds. The observed peak at $(1074, 1089)$ cm $^{-1}$ indicates the presence of specific chemical functionalities, possibly related to $(-C-N, -C-O)$ groups.

3.7 Characterization of the surface of SS304 (AFM analysis)

An AFM analysis was conducted on the SS304 surface to check the existence of an inhibitor film. AFM images and force curves are shown in Fig. 13 after 24 hours of exposure in 1.0 M HCl solution presence and absence SCPs corrosion inhibitors. The mean roughness value of SS304 surface that was exposed to a 1.0 M HCl solution but was not treated with the inhibitor was substantially greater at 300 nm. The acid's corrosive effects over the course of 24 hour rust test period left the SS304 surface with a porous structure and deep fractures, which led to this heightened roughness. However, when the tested inhibitors are applied at the optimum concentration $(16 \times 10^{-6} \text{ M})$, the



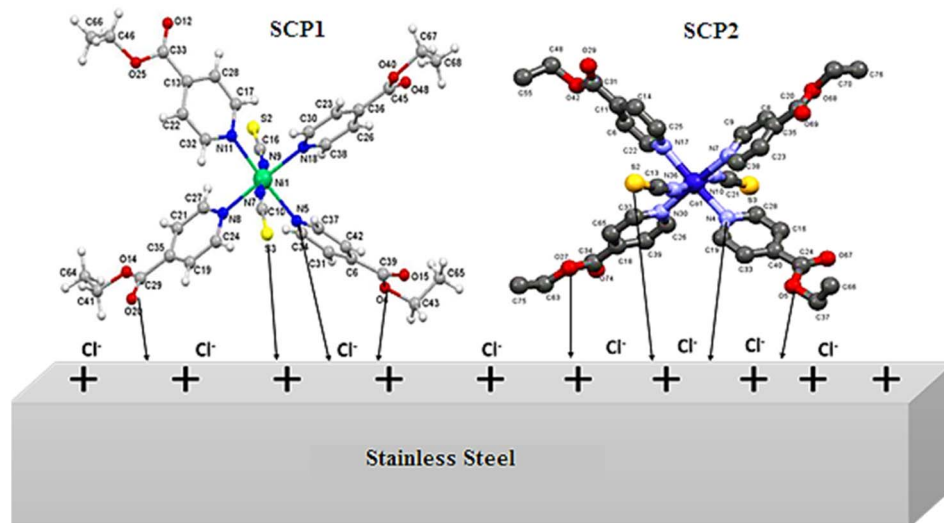


Fig. 14 Mechanism of the adsorption of SCPs on SS304 surface.

average roughness for SCP1 & SCP2 is reduced to 89 & 103 nm, respectively. The test inhibitors effectively maintain hardness of SS304, as seen by the drop in roughness value.⁶²

3.8 Mechanism of adsorption and inhibition

The inhibition efficacy of SCPs compounds on SS304 in 1.0 M HCl can be understood well-known on the molecular size and interface modes of SCPs molecules on SS304 surface Fig. 14. The adsorption mechanism of the SCPs adsorbed on SS304 is generally due to chemical and physical adsorption. The reactive sites present in the molecular structure of the SCPs are responsible for the corrosion inhibition process that depends on the nature and the loading of the metal. The experimental and theoretical methods used in this work justified that the tested SCPs compounds are excellent corrosion inhibitors due to their ability to interact with the atoms of the SS304 surface. The presence of π -electrons and heteroatoms such as oxygen, aromatic unsaturated, and active functional groups promotes the corrosion inhibition of SS304.⁶³ The interaction of the electron-rich aromatic ring with the unpaired electrons of the metal and the inhibitory actions of the SCPs molecules can be explained by the presence of electron-rich oxygen atoms.⁶⁴ It is likely that various interactions can occur, namely: coordination of a metal atom with an unshared electron pair of the inhibitor molecules, sharing of π -electrons of the SCPs in the coordination process, and electrostatic attraction and/or interactions between the negatively charged metal surface and the positively charged SCPs molecules. The protonated form of the adsorbent molecules competes with the aqueous H^+ ion. Nevertheless, upon the release of the H_2 gas, the inhibitors return to their neutral form. The transfer of the unshared electron pairs is reproduced in the unoccupied d-orbital of the metal (retro-donation).⁶⁵ However, this electron transfer generates the accumulation of an additional negative charge on the metal surface. Moreover, this will result in a fresh transfer (back-donation) to the inhibitor molecules' anti-bonding molecular orbitals.⁶⁶

4. Conclusion

The main conclusions drawn from all these studies of SCPs compounds are: the $\eta\%$ of SCPs compounds improves with the rise in inhibitor concentrations whereas it lowered with the increase of temperature. The $\eta\%$ of all composites in altered methods followed the order: SCP1 > SCP2. The adsorption of all the composites on SS304 surface from the acidic solutions conform the Langmuir's adsorption isotherm. Polarization curves indicated that the SCPs act as mixed type inhibitor. SCPs increases R_{ct} values and decreases both C_{dl} and i_{corr} values in 1.0 M HCl solution. FTIR and AFM examination for SS304 surface revealed the attendance of a protective film, which protect SS304 *versus* the destructive media. The experimental finding agrees well with the theoretical calculations.

Conflicts of interest

There are no conflicts to declare.

References

- 1 Y. Gao, T. Yue, W. Sun, D. He, C. Lu and X. Fu, Acid recovering and iron recycling from pickling waste acid by extraction and spray pyrolysis techniques, *J. Cleaner Prod.*, 2021, **312**, 127747.
- 2 I. Nadi, M. Bouanis, F. Benhiba, K. Nohair, A. Nyassi, A. Zarrouk, C. Jama and F. Bentiss, Insights into the inhibition mechanism of 2,5-bis(4-pyridyl)-1,3,4-oxadiazole for carbon steel corrosion in hydrochloric acid pickling via experimental and computational approaches, *J. Mol. Liq.*, 2021, **342**, 116958.
- 3 A. Salmasifar, M. Edraki, E. Alibakhshi, B. Ramezanzadeh and G. Bahlakeh, Combined electrochemical/surface investigations and computer modeling of the aquatic Artichoke extract molecules corrosion inhibition properties



- on the mild steel surface immersed in the acidic medium, *J. Mol. Liq.*, 2021, **327**, 114856.
- 4 J. Sun, H. Tang, C. Wang, Z. Han and S. Li, Effects of Alloying Elements and Microstructure on Stainless Steel Corrosion: A Review, *Steel Res. Int.*, 2022, **93**, 2100450.
 - 5 Q. Sun, M. Yang, Y. Jiang, L. Lei and Y. Zhang, Achieving excellent corrosion resistance properties of 7075 Al alloy via ultrasonic surface rolling treatment, *J. Alloys Compd.*, 2022, **911**, 165009.
 - 6 S. Gudić, A. Nagode, K. Šimić, L. Vrsalović and S. Jozić, Corrosion behavior of different types of stainless steel in PBS solution, *Sustainability*, 2022, **14**, 8935.
 - 7 A. Thakur and A. Kumar, Sustainable inhibitors for corrosion mitigation in aggressive corrosive media: a comprehensive study, *J. Bio-and Tribo-Corrosion*, 2021, **7**, 1–48.
 - 8 A. Zakeri, E. Bahmani and A. S. R. Aghdam, Plant extracts as sustainable and green corrosion inhibitors for protection of ferrous metals in corrosive media: A mini review, *Corros. Commun.*, 2022, **5**, 25–38.
 - 9 A. M. El-Shamy and S. M. Mouneir, Medicinal materials as eco-friendly corrosion inhibitors for industrial applications: A review, *J. Bio-and Tribo-Corrosion*, 2023, **9**, 3.
 - 10 G. Palanisamy, *Corros. Inhib.*, 2019, 1–24.
 - 11 R. Aslam, G. Serdaroglu, S. Zehra, D. K. Verma, J. Aslam, L. Guo, C. Verma, E. E. Ebenso and M. A. Quraishi, Corrosion inhibition of steel using different families of organic compounds: Past and present progress, *J. Mol. Liq.*, 2021, 118373.
 - 12 E. Jin, S. Lee, E. Kang, Y. Kim and W. Choe, Metal-organic frameworks as advanced adsorbents for pharmaceutical and personal care products, *Coord. Chem. Rev.*, 2020, **425**, 213526.
 - 13 S. N. Nangare, S. R. Patil, A. G. Patil, Z. G. Khan, P. K. Deshmukh, R. S. Tade, M. R. Mahajan, S. B. Bari and P. O. Patil, Structural design of nanosize-metal-organic framework-based sensors for detection of organophosphorus pesticides in food and water samples: current challenges and future prospects, *J. Nanostruct. Chem.*, 2021, 1–36.
 - 14 S. F. Fatima, R. Sabouni, R. Garg and H. Gomaa, Recent advances in Metal-Organic Frameworks as nanocarriers for triggered release of anticancer drugs: Brief history, biomedical applications, challenges and future perspective, *Colloids Surf., B*, 2023, 113266.
 - 15 S. Zafari, M. N. Shahrak and M. Ghahramaninezhad, New MOF-Based Corrosion Inhibitor for Carbon Steel in Acidic Media, *Met. Mater. Int.*, 2020, **26**, 25–38.
 - 16 B. Mirzayi, H. Basharnavaz, A. Babapoor, H. Kamali, A. Khodayari and S. Sohrabnezhad, Effects of aluminum terephthalate metal-organic framework and its nanocomposites on the corrosion of AM60B magnesium alloy in ethylene glycol solution containing chloride ions, *Mater. Chem. Phys.*, 2021, **272**, 125056.
 - 17 P. More, K. Jangam, S. Gardi, R. Athavale, F. Choudhary and R. Yamgar, *Grafted Biopolymers as Corrosion Inhibitors: Safety, Sustainability, and Efficiency*, 2023, pp. 89–120.
 - 18 B. Siu, A. R. Chowdhury, Z. Yan, S. M. Humphrey and T. Hutter, Selective adsorption of volatile organic compounds in metal-organic frameworks (MOFs), *Coord. Chem. Rev.*, 2023, **485**, 215119.
 - 19 L. Jiang, Y. Dong, Y. Yuan, X. Zhou, Y. Liu and X. Meng, Recent advances of metal-organic frameworks in corrosion protection: From synthesis to applications, *Chem. Eng. J.*, 2022, **430**, 132823.
 - 20 G. Fekkar, F. Yousfi, H. Elmsellem, M. Aiboudi, M. Ramdani, I. Abdel-Rahman, B. Hammouti and L. Bouyazza, Eco-friendly *Chamaerops humilis* L. fruit extract corrosion inhibitor for mild steel in 1 M HCl, *Int. J. Corros. Scale Inhib.*, 2020, **9**, 446–459.
 - 21 R. S. A. Hameed, M. M. Aljohani, A. B. Essa, A. Khaled, A. M. Nassar, M. M. Badr, S. R. Al-Mhyawi and M. S. Soliman, Electrochemical techniques for evaluation of expired megavit drugs as corrosion inhibitor for steel in hydrochloric acid, *Int. J. Electrochem. Sci.*, 2021, **16**, 210446.
 - 22 C. Verma, H. Lgaz, D. K. Verma, E. E. Ebenso, I. Bahadur and M. A. Quraishi, Molecular dynamics and Monte Carlo simulations as powerful tools for study of interfacial adsorption behavior of corrosion inhibitors in aqueous phase: A review, *J. Mol. Liq.*, 2018, **260**, 99–120.
 - 23 B. Li, S. Ding, S. Guo, W. Su, A. Cheng and J. Hong, A novel isogeometric topology optimization framework for planar compliant mechanisms, *Appl. Math. Model.*, 2021, **92**, 931–950.
 - 24 K. Shoueir, A. M. Wahba, H. El Marouazi and I. Janowska, Performant removal of creatinine using few-layer-graphene/alginate beads as a kidney filter, *Int. J. Biol. Macromol.*, 2023, **242**, 124936.
 - 25 A. R. West, *Solid State Chemistry and its Applications*, John Wiley & Sons, 2022.
 - 26 S. Akhtar, Applications of Atomic Force Microscopy in Corrosion Research, *Recent Dev. Anal. Tech. Corros. Res.*, 2022, 187–201.
 - 27 M. Paraskevaïdi, P. L. Martin-Hirsch and F. L. Martin, ATR-FTIR Spectroscopy Tools for Medical Diagnosis and Disease Investigation, *Nanotechnology Characterization Tools for Biosensing and Medical Diagnosis*, 2018, pp. 163–211.
 - 28 Y. G. Avdeev and Y. I. Kuznetsov, Inhibitory protection of steels from high-temperature corrosion in acid solutions. A review. Part 1, *Int. J. Corros. Scale Inhib.*, 2020, **9**, 394–426.
 - 29 B. Tan, B. Xiang, S. Zhang, Y. Qiang, L. Xu, S. Chen and J. He, Papaya leaves extract as a novel eco-friendly corrosion inhibitor for Cu in H₂SO₄ medium, *J. Colloid Interface Sci.*, 2021, **582**, 918–931.
 - 30 M. Beniken, M. Driouch, M. Sfaira, B. Hammouti, M. Ebn Touhami and M. Mohsin, Kinetic-thermodynamic properties of a polyacrylamide on corrosion inhibition for C-steel in 1.0 M HCl medium: part 2, *J. Bio-and Tribo-Corrosion*, 2018, **4**, 1–13.
 - 31 K. Kashyap, F. Khan, D. K. Verma and S. Agrawal, Effective removal of uranium from aqueous solution by using cerium oxide nanoparticles derived from citrus limon peel extract, *J. Radioanal. Nucl. Chem.*, 2023, **332**, 2435–2445.



- 32 E. Bayol, K. Kayakırlmaz and M. Erbil, The inhibitive effect of hexamethylenetetramine on the acid corrosion of steel, *Mater. Chem. Phys.*, 2007, **104**, 74–82.
- 33 R. Ganjoo, S. Sharma, A. Thakur, H. Assad, P. K. Sharma, O. Dagdag, A. Berisha, M. Seydou, E. E. Ebenso and A. Kumar, Experimental and theoretical study of Sodium Cocoyl Glycinate as corrosion inhibitor for mild steel in hydrochloric acid medium, *J. Mol. Liq.*, 2022, **364**, 119988.
- 34 M. Scendo, The effect of purine on the corrosion of copper in chloride solutions, *Corros. Sci.*, 2007, **49**, 373–390.
- 35 A. S. Fouda, M. A. Ismail, M. A. Khaled and A. A. El-Hossiany, Experimental and computational chemical studies on the corrosion inhibition of new pyrimidinone derivatives for copper in nitric acid, *Sci. Rep.*, 2022, **12**, 1–19.
- 36 J. C. Simoes-Cardoso, N. Yoshimoto and S. Yamamoto, Thermodynamic analysis of polyphenols retention in polymer resin chromatography by van't Hoff plot and isothermal titration calorimetry, *J. Chromatogr. A*, 2019, **1608**, 460405.
- 37 H. Hamani, D. Daoud, S. Benabid, T. Douadi and M. Al-Noaimi, Investigation on corrosion inhibition and adsorption mechanism of azomethine derivatives at mild steel/0.5 M H₂SO₄ solution interface: Gravimetric, electrochemical, SEM and EDX studies, *J. Indian Chem. Soc.*, 2022, **99**, 100330.
- 38 W. J. Hehre, L. Radom, P. V. R. Schreyer and A. J. Pople, *Ab Initio Molecular Orbital Theory*, Wiley-inter Science, NY, 1986.
- 39 A. Shokry, S. Gowid, G. Kharmanda and E. Mahdi, Constitutive models for the prediction of the hot deformation behavior of the 10% Cr steel alloy, *Materials*, 2019, **12**, 2873.
- 40 A. S. Fouda, F. El-Dossoki, E. Hamed and A. El-Hossiany, Inhibition efficiency of erdosteine drug for 304L stainless steel corrosion and its solvation thermodynamic parameters, *Egypt. J. Chem.*, 2022, **65**, 455.
- 41 O. O. Ogunleye, A. O. Arinkoola, O. A. Eletta, O. O. Agbede, Y. A. Osho, A. F. Morakinyo and J. O. Hamed, Green corrosion inhibition and adsorption characteristics of Luffa cylindrica leaf extract on mild steel in hydrochloric acid environment, *Heliyon*, 2020, **6**, e03205.
- 42 M. Prajila and A. Joseph, Controlling the Rate of Dissolution of Mild Steel in Sulfuric Acid Through the Adsorption and Inhibition Characteristics of (4-(4-Hydroxybenzylideneamino)-4H-1,2,4-Triazole-3,5-diyl) dimethanol (HATD), *J. Bio-and Tribo-Corrosion*, 2017, **3**, 1–11.
- 43 A. Al Bahir, Estimation of the performances of creatine and creatinine as eco-friendly corrosion inhibitors for copper in sodium hydroxide solution, *Int. J. Electrochem. Sci.*, 2023, **18**, 100040.
- 44 A. S. Fouda, H. M. Abdel-Wahed, M. F. Atia and A. El-Hossiany, Novel porphyrin derivatives as corrosion inhibitors for stainless steel 304 in acidic environment: synthesis, electrochemical and quantum calculation studies, *Sci. Rep.*, 2023, **13**, 17593.
- 45 B. Xu, W. Yang, Y. Liu, X. Yin, W. Gong and Y. Chen, Experimental and theoretical evaluation of two pyridinecarboxaldehyde thiosemicarbazone compounds as corrosion inhibitors for mild steel in hydrochloric acid solution, *Corros. Sci.*, 2014, **78**, 260–268.
- 46 N. Dkhireche, M. Galai, Y. El Kacimi, M. Rbaa, M. Ouakki, B. Lakhri and M. E. Touhami, New quinoline derivatives as sulfuric acid inhibitor's for mild steel, *Anal. Bioanal. Electrochem.*, 2018, **10**, 111–135.
- 47 M. Abdallah, S. A. Ahmed, H. M. Altass, I. A. Zaafarany, M. Salem, A. I. Aly and E. M. Hussein, Competent inhibitor for the corrosion of zinc in hydrochloric acid based on 2, 6-bis-[1-(2-phenylhydrazono) ethyl] pyridine, *Chem. Eng. Commun.*, 2019, **206**, 137–148.
- 48 K. Cherrak, M. El Massaoudi, H. Outada, M. Taleb, H. Lgaz, A. Zarrouk, S. Radi and A. Dafali, Electrochemical and theoretical performance of new synthesized pyrazole derivatives as promising corrosion inhibitors for mild steel in acid environment: Molecular structure effect on efficiency, *J. Mol. Liq.*, 2021, **342**, 117507.
- 49 A. O. James, N. C. Oforka and O. K. Abiola, Inhibition of acid corrosion of mild steel by pyridoxal and pyridoxol hydrochlorides, *Int. J. Electrochem. Sci.*, 2007, **2**, 278.
- 50 B. Xu, W. Yang, Y. Liu, X. Yin, W. Cong and Y. Chen, Experimental and theoretical evaluation of two pyridinecarboxaldehyde thiosemicarbazone compounds as corrosion inhibitors for mild steel in hydrochloric acid solution, *Corros. Sci.*, 2014, **78**, 260–268.
- 51 M. E. Mashuga, L. O. Olasunkanmi, C. Verma, E.-S. M. Sherif and E. E. Ebenso, Experimental and computational mediated illustration of effect of different substituents on adsorption tendency of phthalazinone derivatives on mild steel surface in acidic medium, *J. Mol. Liq.*, 2020, **305**, 112844.
- 52 A. Rochdi, O. Kassou, N. Dkhireche, R. Tour, M. El Bakri, M. E. Touhami, M. Sfaira, B. Mernari and B. Hammouti, Inhibitive properties of 2,5-bis(n-methylphenyl)-1,3,4-oxadiazole and biocide on corrosion, biocorrosion and scaling controls of brass in simulated cooling water, *Corros. Sci.*, 2014, **80**, 442–452.
- 53 Z. Z. Wang, Y. Y. Li and G. A. Zhang, Inhibitive effects of inhibitors on the galvanic corrosion between N80 carbon steel and 13Cr stainless steel under dynamic supercritical CO₂ conditions, *Corros. Sci.*, 2019, **146**, 121–133.
- 54 S. A. Al Kiey, H. R. M. Rashdan and M. E. El-Naggar, Insight into mitigation of corrosion behavior of novel chalcone derivative for AZ91 Mg alloy in saline solution: synthesis, characterization, electrochemical and adsorption studies, *J. Electroanal. Chem.*, 2023, **934**, 117304.
- 55 M. A. Khaled, M. A. Ismail, A. A. El-Hossiany and A. E.-A. S. Fouda, Novel pyrimidine-bichalcophene derivatives as corrosion inhibitors for copper in 1 M nitric acid solution, *RSC Adv.*, 2021, **11**, 25314–25333.
- 56 T. Koopmans, Über die Zuordnung von Wellenfunktionen und Eigenwerten zu den Einzelnen Elektronen Eines Atoms, *Physica*, 1934, **1**, 104–113.
- 57 W. Gao, C. Addiego, H. Wang, X. Yan, Y. Hou, D. Ji, C. Heikes, Y. Zhang, L. Li and H. Huyan, Real-space charge-density imaging with sub-ångström resolution by



- four-dimensional electron microscopy, *Nature*, 2019, **575**, 480–484.
- 58 M. Abdallah, H. M. Altass, A. S. Al-Gorair, J. H. Al-ahemi, B. A. A. L. Jahdaly and K. A. Soliman, Natural nutmeg oil as a green corrosion inhibitor for carbon steel in 1.0 M HCl solution: Chemical, electrochemical, and computational methods, *J. Mol. Liq.*, 2021, **323**, 115036.
- 59 J. S. M. Anderson, J. Mellin and P. W. Ayers, Conceptual Density-Functional Theory for General Chemical Reactions, Including Those That Are Neither Charge- nor Frontier-Orbital-Controlled. 1. Theory and Derivation of a General-Purpose Reactivity Indicator, *J. Chem. Theory Comput.*, 2007, **3**, 358–374.
- 60 O. A. Elgyar, A. M. Ouf, A. El-Hossiany and A. E. A. S. Fouda, The inhibition action of viscum album extract on the corrosion of carbon steel in hydrochloric acid solution, *Biointerface Res. Appl. Chem.*, 2021, **11**, 14344–14358.
- 61 H. Wang, S. Sharma, A. Pailleret, B. Brown and S. Nešić, Investigation of corrosion inhibitor adsorption on mica and mild steel using electrochemical atomic force microscopy and molecular simulations, *Corrosion*, 2022, **78**, 990–1002.
- 62 C. Verma, V. S. Saji, M. A. Quraishi and E. E. Ebenso, Pyrazole derivatives as environmental benign acid corrosion inhibitors for mild steel: Experimental and computational studies, *J. Mol. Liq.*, 2020, **298**, 111943.
- 63 C. Verma, A. Thakur, R. Ganjoo, S. Sharma, H. Assad, A. Kumar, M. A. Quraishi and A. Alfantazi, Coordination bonding and corrosion inhibition potential of nitrogen-rich heterocycles: Azoles and triazines as specific examples, *Coord. Chem. Rev.*, 2023, **488**, 215177.
- 64 H. S. Aljibori, O. H. Abdulzahra, A. J. Al Adily, W. K. Al-Azzawi, A. A. Al-Amiery and A. A. H. Kadhum, Corrosion inhibition effects of concentration of 2-oxo-3-hydrazoneindoline in acidic solution, exposure period, and temperature, *Int. J. Corros. Scale Inhib.*, 2023, **12**, 438–457.
- 65 W. Guo, M. Talha, Y. Lin, Y. Ma and X. Kong, Effect of phosphonate functional group on corrosion inhibition of imidazoline derivatives in acidic environment, *J. Colloid Interface Sci.*, 2021, **597**, 242–259.
- 66 M. Beniken, S. Daoui, S. A. Mrani, F. Benhiba, N. Benchat, A. Zarrouk and M. Taleb, Electrochemistry evaluation and quantum corroboration with surface analysis of potential anticorrosive of two new pyridazine derivatives for mild steel in 1 M HCl solution, *Colloids Surf., A*, 2023, **673**, 131699.

